Nano World Journal

https://doi.org/10.17756/nwj.2023-s5-055

Research Article

Open Access

Heat Transfer of Crossflow of MHD Williamson Fluid Over a Porous Shrinking Surface Consisting of CuO-TiO_2/Water Hybrid Nanofluid with Thermal Radiation, Buoyancy, and Heat Source/Sink Impacts

R. Mehta[1], S. Jangid[1], M.K. Sharma[2*] and A. Bhatnagar[3]

[1]*Department of Mathematics and Statistics, Manipal University, Jaipur, Rajasthan, India*

[2]*Department of CCE, Manipal University, Jaipur, Rajasthan, India*

[3]*Department of Information Technology, Manipal University, Jaipur, Rajasthan, India*

[*]Correspondence to:
M.K. Sharma
Department of CCE,
Manipal University,
Jaipur, Rajasthan, India.
E-mail: M0918.sharma@gmail.com

Received: October 20, 2023
Accepted: December 22, 2023
Published: December 28, 2023

Citation: Mehta R, Jangid S, Sharma MK, Bhatnagar A. 2023. Heat Transfer of Crossflow of MHD Williamson Fluid Over a Porous Shrinking Surface Consisting of CuO-TiO_2/Water Hybrid Nanofluid with Thermal Radiation, Buoyancy, and Heat Source/Sink Impacts. *NanoWorld J* 9(S5): S293-S304.

Copyright: © 2023 Mehta et al. This is an Open Access article distributed under the terms of the Creative Commons Attribution 4.0 International License (CCBY) (http://creativecommons.org/licenses/by/4.0/) which permits commercial use, including reproduction, adaptation, and distribution of the article provided the original author and source are credited.

Published by United Scientific Group

Abstract

The area of this research is to inspect the Williamson fluid flow through a rotating stagnation point toward a reducing permeable wall included by a CuO-TiO_2/H_2O (Copper oxide-Titanium dioxide/Water). The form considerations, as well as the thermal radiation, Joule heating, buoyancy force, and heat generation/absorption parameters, are considered. The enclosed boundary layers are stream-wise by the shrinking sheet. PDEs are renovated into ODEs with the appropriate transformations. For unique values of relevant parameters, the transmogrified system of ODEs is calculated using the MATLAB tool with bvp4c. The friction factor increased when GT and SA raised, but increasing W and Mn had the reverse effect. Improving Q and Ec increased the heat transference rate, but growing Nr had the reverse effect.

Keywords

Williamson fluid, Thermal Radiation, Joule heating, Shrinking/stretching sheet

Introduction

In the latest generations, investigators and scientists have focused their impressions on the inquiry of hybrid nanofluids, a novel form of fluid. Hybrid nano-liquids are fluids with a better thermos-conduction impact than nano liquids and regular liquids. The diffusion of twice kinds of nanoparticles in the carrier liquid produces hybrid nano-liquids. The hybrid nanoparticle energy transition has been developed mechanically to upsurge heat transmission in numerous engineering and industrial processes. In evaluation to the standard and base liquids, the hybrid nano-liquid exhibits a high thermal reliability, heat pumps, heat capacitances, microelectronics, digital freezing, car heaters, atomic control positions, coolant in lettering and engine apparatuses, nano-drag consignments, vehicle control formation, remedy for cancer, and other usages of hybrid nanofluid in manufacturing and engineering machines. Many academics and scientists are doing surveys on hybrid nano-liquids as a significance of their important applications.

Once an electrical current flows through a conductor and creates heat, it is called a joule heating effect. The Joule heating impact is utilized in a variety of gadgets and industrial operations. The Joule heating effects are used in food dispensation, scanning electron microscopy, infrared-thermal descriptions, electrical radiative space heaters, vivacious light bulbs, test centre aquatic baths, electrical tabletop hotplates, garments irons, bonding irons, spiracle heaters, hair dryers, and container heaters. For a variety of exponents and amplitudes β, the

parallel explanation of the Prandtl border layer equalization telling bounded wall movements and symmetrical free-shear streams determined by rotating velocities u_∞ (y) = $\beta_A y^\alpha$ is determined by Weidman et al. [1]. The equations' asymptotic analysis reveals that $\alpha < -1$ there are no similar solutions with adequate algebraic decay. Explanations discovered at $\alpha = -1/2$ and $\alpha = 1$ link to an airy function wall jet and unvarying two-dimensional Couette flow for wall-bounded flow. Labib et al. [2] investigated the forced convective heat transference of nano-liquids via a twice-phase mix model, providing a new notion of heat transfer augmentation. Madhesh and Kalaiselvam [3] explored the impact of thermos-features of forced convection, thermos-conductivity, and heat transference rate on the heat transport activity of hybrid nanofluid (copper-titanium hybrid nanocomposite/water) flow via the tubular heat exchanger. Sarkar et al. [4] provided a review of recent research on hybrid nanofluids' production, thermophysical properties, heat transmission, pressure fall features, potential uses, and obstacles. The mathematical simulation of mixing convective heat transference coefficient in a 2D trapezoidal lid-driven container loaded with nano-fluids warmed downward was studied by Kareem et al. [5]. The research on synthesizing, thermo-physical features, heat transmission rate, hydrodynamic action, and fluid flow features was published by researchers Babu et al. [6] on various hybrid nanofluids. Nabil et al. [7] reviewed past work on the thermophysical features of hybrid nano-liquids/nano-lubricants, including preparation methods, instruments, development and advancement, and hybrid effectiveness in terms of heat transference and pressure drop. Sidik et al. [8] highlighted recent advancements in hybrid nanofluid fabrication methods, issues impacting its stability, approaches for improving thermal characteristics and existing hybrid nanofluid uses.

Hydromagnetic is a division of physics dealing with the performance of magneto and electrically leading liquids such as seawater, fluid metallic element, electrolytes, and plasma. Hydromagnetic is used in a variation of technical and industrial usages, counting creators and electrical strainers, heat swapper, power pumps, reactor freezing, electricity production, plasma, MHD sensor, and magnetic drug marking, crystal amplification, and so on. Numerous academics and scholars are fascinated in learning behavior caused by the magnetic effect, mostly in the condition of boundary layer flow matters. Esfe et al. [9] proposed a system based on earlier studies to guess the thermal conductivity of hybrid nano-liquids including carbon nanotubes (MWCNT–MgO/water–EG nano-liquids). An investigation studied by Vasanthakumari and Pondy [10] of stable 2D laminal boundary layer flow of an incompressible, viscid nanofluid with hydromagnetic, considering heat production and suction. Mostafazadeh et al. [11] used radiation and buoyancy effects to model heat transference and laminal movement of a nanofluid in an erect channel. They used single- and two-phase methods with given surface temperature settings and prescribed surface heat flux numbers. Waini et al. [12] investigated the unsteady flow and heat transmission through an extended/shrinked surface in a hybrid nanofluid. Khan et al. [13] used a thin revolution body made of molybdenum-disulfide graphene oxide generalised hybrid nano-liquids implanted in a porous medium to handle the buoyancy flow. Through a tiny needle, Khan et al. [14] inspected the magneto Williamson liquid uniting titanium alloy particles. Qureshi [15] inspected the heat transference and entropy of a time-independent Williamson nano-liquid flow over a stretchy flat surface (an irregular flowing form) in prospect of a single-phase model descripting for Cu-water and TiO_2-water nano-liquids. Asadi et al. [16] published an investigation all earning on the representation, steadiness, and dynamic viscosity of CuO-TiO_2/water hybrid nanofluids, in which the chemical, microscopic, and surface construction of CuO and TiO_2 nanosized elements were investigated with X-ray deflection, Fourier-transform infrared spectroscopy, and Turf emission skimming electron microscopy assessments. The flow, heat transference, and entropy of electrically conducting hybrid nanofluids (Copper Ethylene glycol (Cu-EG) nano-fluid and Ferro-Copper Ethylene glycol (Fe_3O4-Cu-EG) over the horizontal penetrable stretch sheet were inspected by Aziz et al. [17]. Chu et al. [18] used Lorentz's forces on mixed convection boundary-layer flow and heat radiation via an upright cylinder to capture water as a normal fluid with interruption of dual forms of hybrid nanosized particles, i.e., molybdenum disulfide and graphene oxide. Nisar et al. [19] inspected the nonlinear influence of radiation on hybrid alloy nanoparticle magnet flow in both stream-wise and cross flow. Date et al. [20] employed template-assisted low-cost procedures to produce 3D CuO/TiO_2 hybrid heterostructure nanorod formalizes with noble-metal-free structure as the photo Fenton-like catalytic agent for dye degression.

Enhancements in fluid heat transference amount have resentful the attention of investigators and technologists because of their many applications in the medicinal, manufacturing, and technological fields. Heat transference via the hybrid nano liquid has a wide range of applications in mechanism and engineering discipline, chemical study, and biology, including food dispensation, protecting resources, polymers, solar energy, and reactor fluidizations, freezing of microchips, solar water boiler, geothermal power removal, beaker creating, and hydraulic disruptions, among others. Because of these numerous applications, numerous investigators have investigated the influence of heat evolution on numerous flow situations. The hydrodynamic performance of a laminar mixing convective flow of an Ag-TiO_2/water hybrid nano-liquid in the entry area of a flat annulus with a thermal boundary limit of constant heat flux at the interior wall and an adiabatic external wall has been inspected numerically by Albeshri et al. [21]. Ramzan et al. [22] focused on the analysis of the hydromagnetic flow of an Ag-MgO/water hybrid nano-liquid under slipping circumstances through a spreading surface. Muhammad et al. [23] investigated the unsteady squeezed flow of hybrid nano-liquid (CNTs + CuO) and nano-liquid (CNTs) with base fluid water, as well as melting impact, viscous dissipation, entropy production, and Bejan number. Othman et al. [24] conducted research into the flow and heat transference characteristics of a hybrid nano-liquid containing CNTs on a porous exponential diminishing surface, in addition to the impacts of a magneto field and a heat source/sink. Khan et al. [25] inspected the Williamson fluid flow over a rotating stagnation point near a shrinking or extending porous wall included by CuO-TiO_2/hybrid nano-

liquid. Almaneea [26] investigated the use of Cu-Al_2O_3/Glycerine. hybrid nanoparticles to improve energy and mass transmission in hydromagnetic Williamson fluid.

The crossflow caused via non-Newtonian fluid through a stretchy or reducing sheet is explored close a rotating stagnation point in the attendance of form variables, according to existing research. Primary objective of this work is to fill this gap the authors examine the Williamson fluid flow transporting hybrid nano liquid (CuO-TiO_2/water) over a reducing/extending sheet while accounting for radiation, Joule heating, buoyancy force, and heat generation/absorption parameters with the extended work of [25]. For a particular range of shrinking/stretching parameters, the similarity in many outcomes was discovered. The numerical solutions obtained using the present recommended model for hybrid nanofluid are thought to open up new possibilities for scientists studying heat transfer. For different settings, the skin friction and Nusselt number have been calculated. Furthermore, for various parameters, the behavior of hybrid nano-liquid velocity and temperature is estimated in graphic form. However, research into this flow over a reducing/extending sheet has not yet started. We can be confident that the results of our computational work are applied to any real-time issues in a variety of thermal engineering fields, including energy production, heating and cooling systems, and the design of new thermal systems, medical science like as cancer therapy, industries, etc.

Experimentation

Mathematical formulation

Governing relations for shear thinning Williamson fluid [25] are:

$$S = -PI + \tau, \quad \text{here } \tau = \left(\mu_\infty + \frac{\mu_0 - \mu_\infty}{1 - \Gamma\beta}\right) A_1$$

Where, P locations for pressure, I look for identity vector, τ suggestions the extra stress tensor, μ_0 and μ_∞ exhibition for limit viscidness at 0 and ∞ shear rate respectively, A_1 offerings the Rivilin—Erickson tensor and β is $\sqrt{1/2}\pi, \pi = trace(A_1)^2$.

Here, we deliberate the case for which:

$$\mu_\infty = 0, \Gamma\beta < 1.$$

$$\tau = \left(\frac{\mu_0}{1 - \Gamma\beta}\right) A_1 \text{ or } \tau = \mu_0 (1 + \Gamma\beta) A_1.$$

Over a porous shrinking/extending surface, a 2D incompressible, viscid, and laminal boundary layer crossflow and heat transference of a Williamson hybrid nano-liquid is addressed. The numerous form parameters, as well as Buoyancy force, Joule heating, and heat generation/absorption parameter with heat radiation, are considered in the current investigation. The hybrid nano-liquid is collected of two different nanoelements CuO and TiO_2 combined with a standard fluid water. Thermal equilibrium is assumed for the hybrid nanofluid's characteristics. Figure 1 depicts a simplified representation of the flow formation model with the nanosized particles form in

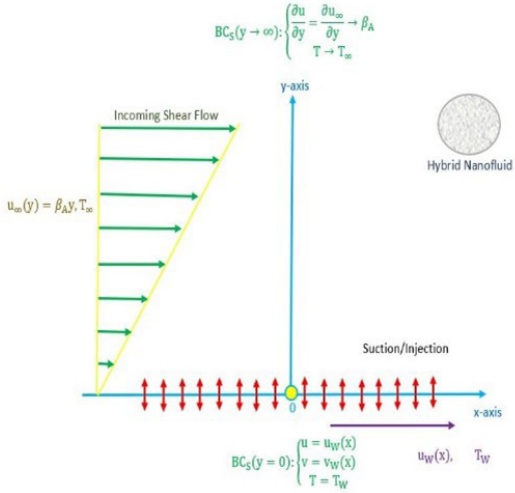


Figure 1: Physical illustration of the flow issue combined with the reference frame.

the cartesian arrangement, where the coordinate X-axis runs similar to the sheet's surface and the coordinate Y-axis is erect to it. The flow is continued infinitely along the Z-axis (spanwise) in the schematic picture, indicating that it is established. As a result, we search for various outcomes with velocity profiles that are not constrained by the direct X-axis. As the sheet's surface is strained and narrowed in +ve and -ve X-axis with an adjustable velocity, $u_w(x) = \beta_A^{2/3} \nu_{Bf}^{1/3} x^{1/3} \lambda_A$, where λ_A is the unvarying stretching/shrinking parameter. Furthermore, the +ve and -ve amount of the parameter λ_A cause the sheet's surface to stretch and shrink, respectively, whilst the zero value relates to a stationary sheet.

Furthermore, the nonuniform movement of the free-stream or ambiance from the sheet (no viscous flow) is assumed to be modelled by [1, 25].

$$u_\infty(y) = \beta_A y \tag{1}$$

Where, β_A is a positive constant that might be anything. Also, assume that $v_w(x)$ represents transpiration or permeable velocity, and that $v_w(x) < 0$ represents injection or blowing, and $v_w(x) > 0$ represents suction, respectively. T_w and T_∞ stand for surface continuous temperature and far-field (no viscous flow) temperature, respectively. The required leading relations for the investigated energy and fluid flow dynamics, under the stated caveat, are as follows [15, 22, 25].

Equation of continuity

$$\frac{\partial u}{\partial x} + \frac{\partial v}{\partial y} = 0 \tag{2}$$

Equation of velocity

$$\rho_{hbnf}\left(u\frac{\partial u}{\partial x} + v\frac{\partial u}{\partial y}\right) = \mu_{hbnf}\left(\frac{\partial^2 u}{\partial y^2} + \sqrt{2}\Gamma\frac{\partial u}{\partial y}\frac{\partial^2 u}{\partial y^2}\right) + \sigma_{hbnf}B_0^2 u + g_0(\rho\beta_T)_{hbnf}(T - T_\infty) \tag{3}$$

Equation of temperature

$$\left(\rho C_p\right)_{hbnf}\left(u\frac{\partial T}{\partial x}+v\frac{\partial T}{\partial y}\right)= k_{hbnf}\frac{\partial^2 T}{\partial y^2}-\frac{\partial q_r}{\partial y}+\sigma_{hbnf}B_0^2u^2+Q_0\left(T-T_\infty\right) \quad (4)$$

The physical boundary conditions [1, 19] for the present condition are as tracks:

$$u=\lambda_A u_w(x); v=v_w(x) T=T_w(x) \text{ at } y=0$$

$$\frac{\partial u}{\partial y}\to\frac{\partial u_\infty}{\partial y}; T\to T_\infty \text{ at } y=\infty \quad (5)$$

The factors of speed in the reliable directs of Y-axis and X-axis are denoted by v (m/s) and u (m/s), respectively, here T (K) is the fluid's temperature and Γ is the time constant. Furthermore, *hbnf* views for hybrid nano-liquid, *Bf* depicts for base fluid, $\left(\tilde{n}C_p\right)_{hbnf}$ depicts the heat capacity of the hybrid nano-liquid, B_0 (Tesla) stands the strength of magnetic field, the gravitational acceleration is g_0,σ_{hbnf} depicts the electrical conductivity, β_{Thbnf} depicts for the thermal expansion coefficient, k_{hbnf} depicts the thermal conductivity of the hybrid nano-liquid, ρ_{hbnf} depicts the density of the hybrid nano-liquid, and μ_{hbnf} denotes the hybrid nano-liquid's dynamic viscosity.

Here, C_p depicts for the specific heat at continuous pressure, $\phi_{CuO}=\phi_1$ stands for the volume fraction of CuO, $\phi_{TiO_2}=\phi_2$ stands the volume fraction of TiO_2 and k_{Bf}, μ_{Bf}, ρ_{Bf} and σ_{Bf} stand for the thermal conductivity, dynamic viscosity, density, and electric conductivity of the regular fluid, respectively. The subscripts Bf, CuO, and TiO_2 denote the amounts of base fluid, copper oxide nanoparticles, and titanium dioxide nanoparticles, respectively. Therefore, table 1 holds data of the working pure fluid as well as twice nanomaterials. Table 2 shows the (TiO_2-CuO/water) hybrid nanoparticles' physical properties. Table 3 also highlights the several shape feature coefficients and different figures of nanoparticles.

The next to last term in relation (4), where q_r shows the radiative heat flux and is described using the Rosseland estimate, denotes thermal radiation [15, 25].

$$q_r=\frac{-4\sigma^*}{3k^*}\frac{\partial T^4}{\partial y} \quad (6)$$

Here, σ^* is the Stefan-Boltzmann constant and k^* corresponds to the coefficient of mean absorption. Now, with the Taylor series for the term T^4 at T_∞ and disregarding the high-order terms in estimation, the last form may be found. Where T4 is a linear connection of temperature through Taylor's series expansion about T_∞ and forgetting advanced terms, thus:

$$T^4\approx 4T_\infty^3T-3T_\infty^4 \quad (7)$$

In the existing work, we may solve our work by taking the next dimensionless quantities [1, 25].

Table 1: The formulae and limits for the hybrid nano-liquid in the system of equations.

Thermal properties	Hybrid nanofluid
Thermal Diffusivity	$\alpha_{hbnf}=\frac{k_{hbnf}}{\left(\rho C_p\right)_{hbnf}}$
Viscosity	$\frac{\mu_{hbnf}}{\mu_{Bf}}=\frac{1}{\left(1-\phi_{CuO}-\phi_{TiO_2}\right)^{2.5}}$
Density	$\frac{\rho_{hbnf}}{\rho_{Bf}}=\phi CuO\frac{\rho_{CuO}}{\rho_{Bf}}+\phi_{TiO_2}\frac{\rho_{TiO_2}}{\rho_{Bf}}+\left(1-\phi_{CuO}-\phi_{TiO_2}\right)$
Heat Capacity	$\frac{\left(\rho C_p\right)_{hbnf}}{\left(\rho C_p\right)_{Bf}}=\phi_{CuO}\frac{(\rho Cp)_{CuO}}{(\rho Cp)_{Bf}}+\phi_{TiO_2}\frac{\left(\rho C_p\right)_{TiO_2}}{\left(\rho C_p\right)_{Bf}}+\left(1-\phi_{CuO}-\phi_{TiO_2}\right)$
Thermal Expansion	$\frac{(\rho\beta_T)_{hbnf}}{(\rho\beta_T)_{Bf}}=\phi_{CuO}\frac{(\rho\beta_T)_{CuO}}{(\rho\beta_T)_{Bf}}+\phi_{TiO_2}\frac{(\rho\beta_T)_{TiO_2}}{(\rho\beta_T)_{Bf}}+\left(1-\phi_{CuO}-\phi_{TiO_2}\right)$
Thermal Conductivity	$k_{hbnf}=\frac{k_{TiO_2}+(M-1)k_{nf}-(M-1)\phi_{TiO_2}\left(k_{nf}-k_{TiO_2}\right)}{k_{TiO_2}+(M-1)k_{nf}+\phi_{TiO_2}\left(k_{nf}-k_{TiO_2}\right)}k_{nf}$ Where, $k_{nf}=\frac{k_{CuO}+(M-1)k_{Bf}-(M-1)\phi_{CuO}\left(k_{Bf}-k_{CuO}\right)}{k_{CuO}+(M-1)k_{Bf}+\phi_{CuO}\left(k_{Bf}-k_{CuO}\right)}k_{Bf}$
Electrical Conductivity	$\sigma_{hbnf}=\frac{\sigma_{TiO_2}+(M-1)\sigma_{nf}-(M-1)\phi_{TiO_2}\left(\sigma_{nf}-\sigma_{TiO_2}\right)}{\sigma_{TiO_2}+(M-1)\sigma_{nf}+\phi_{TiO_2}\left(\sigma_{nf}-\sigma_{TiO_2}\right)}\sigma_{nf}$ Where, $\sigma_{nf}=\frac{\sigma_{CuO}+(M-1)\sigma_{Bf}-(M-1)\phi_{CuO}\left(\sigma_{Bf}-\sigma_{CuO}\right)}{\sigma_{CuO}+(M-1)\sigma_{Bf}+\phi_{CuO}\left(\sigma_{Bf}-\sigma_{CuO}\right)}\sigma_{Bf}$

$$u = \beta_A^{2/3} v_{Bf}^{1/3} x^{1/3} f'(\eta), \eta = \beta_A^{1/3} v_{Bf}^{1/3} x^{-1/3} y, \theta(\eta) = \frac{T - T_\infty}{T_w - T_\infty}$$

and

$$v = -(1/3)\beta_A^{1/3} v_{Bf}^{2/3} x^{-1/3}\left[2f(\eta) - \eta f'(\eta)\right]. \quad (8)$$

The prime stands for differentiation about the pseudo-similarity variables, and the nonuniform motion at the sheet's porosity shrinking/stretching surface is labelled as:

$$v_w(x) = -(2/3)\beta_A^{1/3} v_{Bf}^{2/3} x^{-1/3} S_A \quad (9)$$

Here, S_A denotes the mass flux feature, with $S_A > 0$ and $S_A < 0$ consistent to suction and blowing, correspondingly, and $S_A = 0$ corresponding to an impenetrable sheet surface.

With the similarity variations equation 8, produce controlling equations 2 to 4, where the continuity relation 2 is totally satisfied and the other equations accept the non-dimensional form exposed below:

$$3\frac{\mu_{hbnf}/\mu_{Bf}}{\rho_{hbnf}/\rho_{Bf}}(1 + Wf'')f'' - (f')^2 + 2ff'' - 3\frac{\sigma_{hbnf}/\sigma_{Bf}}{\rho_{hbnf}/\rho_{Bf}}Mnf' + 3\frac{(\rho\beta_T)_{hbnf}/(\rho\beta_T)_{Bf}}{\rho_{hbnf}/\rho_{Bf}}G_T\theta = 0 \quad (10)$$

$$\frac{3\theta''}{Pr(\rho C_p)_{hbnf}/(\rho C_p)_{Bf}}\left(\left(k_{hbnf}/k_{Bf}\right) + (4/3)Nr\right) + 2f\theta' + 3\frac{\sigma hbnf/\sigma Bf}{(\rho C_p)_{hbnf}/(\rho C_p)_{Bf}}EcMn(f')^2 + \frac{3}{(\rho C_p)_{hbnf}/(\rho C_p)_{Bf}}Q\theta = 0 \quad (11)$$

With the limit circumstances in issue:

$$f(0) = S_A, f'(0) = \lambda_A, \theta(0) = -1 \text{ at } \eta = 0$$
$$f''(\infty) \to 1, \theta(\infty) \to 0 \text{ at } \eta \to \infty \quad (12)$$

The Williamson fluid parameter (W), Hartmann number (Mn), local Grashof temperature number (GT), Eckert parameter (Ec), heat generation/absorption parameter (Q), Prandtl parameter (Pr), and radiation parameter (Nr) are all terms used to describe the participation of non-dimensional limits in equation 10 and equation 12. These variables are stated numerically as:

$$W = \sqrt{2}\Gamma\beta_A,\ Mn = \frac{\sigma_{Bf}B_0^2 x}{\rho_{Bf}\beta_A^2},$$

$$G_T = \frac{g_0(\beta_T)_{Bf}(T_w - T_\infty)}{\beta_A^{4/3} v_{Bf}^{2/3} x^{-1/3}},$$

$$Ec = \frac{\beta_A^{4/3} v_{Bf}^{1/3} x^{1/3}}{(C_p)_{Bf}(T_w - T_\infty)},$$

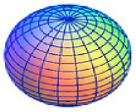
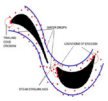
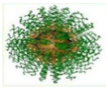
$$Q = \frac{Q_0 \beta_A^{-2/3} v_{Bf}^{2/3} x^{2/3}}{(\rho C_p)_{Bf}},$$

$$Pr = \frac{v_{Bf}}{\alpha_{Bf}}, \text{ and } Nr = \frac{4\sigma_A^* T_\infty^3}{3k_{Bf}k_A^*}.$$

Table 2: (TiO_2-CuO/water) hybrid nanoparticles' physical properties.

Physical features	Water	CuO	TiO_2
ρ	997.1	6510	4250
C_P	4179	540	686.2
K	0.613	18	8.9538
σ	0.5 x 10^{-6}	5.96 x 10^7	2.38 x 10^6
β_T	21 x 10^5	0.85 x 10^5	0.9 x 10^5
P_r	6.2	-	-

Table 3: The form factor coefficient (M) for a variety of nanoparticle shapes.

Nanosized particles	Figure	Figure factor (M)
Sphere		3
Cylinders		4.9
Blades		8.6
Lamina		16.1576

The skin friction and heat transference rate are the physical parameters of engineering significance, and they are described as tracks: The skin frictions $C_f = \frac{\tau_w}{\rho_{Bf}u_w^2}$, and the Nusselt number is well-defined as $Nu_x = \frac{xq_w}{k_{Bf}(T_w - T_\infty)}$.

The shear stress τ_w is expected by

$$\tau_w = \mu_{hbnf}\left(\frac{\partial u}{\partial y}\left(1 + \frac{\Gamma}{\sqrt{2}}\frac{\partial u}{\partial y}\right)\right)_{y=0}, \text{ we get}$$

$$C_f \,\mathrm{Re}_x^{1/2} = \mu_{hbnf}/\mu_{Bf}\left[f''(0) + (W/2)(f''(0))^2\right]$$

The heat transference rate q_w is assumed by

$$q_w = -k_{hbnf}\left(\frac{\partial T}{\partial y}\right)_{y=0} + (q_r)_{y=0}, \text{ we get}$$

$$Nu_x \,\mathrm{Re}_x^{-1/2} = -\left[\left(k_{hbnf}/k_{Bf}\right) + (4/3)Nr\right]\theta'(0)'$$

Where, $Re_x = \frac{xu_w}{v_{Bf}}$ is the Reynolds number.

Results and Discussion

Some of the most essential uses of the current physical

model are examined in depth. The stretching sheet is used to cool incessant floorings or filaments by dragging them over a calm liquid in the fields of polyvinyl chloride, pipe manufacture, wiredrawing, metal forming, hot progressing, and so on. In manufacturing uses, the problematic heat transference flow linked to the extending surface is critical, for example, in metallurgical procedures such as copper wire tinning and annealing, illustration of incessant filaments, and producing of rubber and plastic sheets through calm fluids, fibre revolving and continuous freezing, and crystal rising, as well as a wide range of other engineering development.

The influence of numerous elaborated physical numbers volume fractions of nanomaterials ϕ_{TiO_2} and ϕ_{CuO}, suction parameter S_A, shrinking parameter λ_A, Weissenberg number W, radiation parameter Nr, Hartmann number Mn, local Grashof temperature number G_T, Eckert number Ec, heat generation/absorption parameter Q, and Prandtl number Pr on momentum profile, temperature profile, skin friction f" (η) in the entire boundary layer area, skin friction, and heat transference rate is confined in the arrangement of numerous images for the water-based CuO-TiO_2 fluid from figures 2 to figure 27. Throughout the text, we have used the paucity amounts of the constraints, such as $\phi_{TiO_2} = \phi_2 = 0.035$ and $\phi_{CuO} = \phi_1 = 0.025$, S_A = 2.00, λ_A = -0.1, W = 0.1, Nr = 0.1, Mn = 0.5, G_T = 0.1, Ec = 0.1, Q = 0.1, and Pr = 6.2 to compute the results. Following the simulations, we discovered that the impact of form factors on gradients, motion profiles, and temperature profiles. As a result, we created three figures (Figure 2 to figure 4) to show the effect of various form parameters on motion profiles, gradient, and temperature formulations, whereas the relax of the pictures were created for the blades M = 8.6.

Figure 2 to figure 4 show the influence of various form factors M and mass suction S_A on dimensionless velocity, shear stress, and temperature versus the pseudo-similarity variable η. When M increased, the solution drops in velocity and shear stress formulations while increasing in temperature formulation. Furthermore, for both velocity and shear stress profiles, solutions are lower for the figure lamina M = 16.1576 and greater for the shape sphere M = 3, although the opposite trend is seen in temperature formulation. More specifically, the temperature graphs, the separate influence of form parameters can increase thermal conductivity and enhance heat transference rate, giving sureness that the temperature formulations are created higher.

Figure 5 and figure 6 show the effect of W on f′(η) and f″(η) dispersed throughout the full spatial domain for solution versus the pseudo-similarity variable η, respectively. The Williamson number is the fraction of relaxation time to process time, a decrease in the process's particular time will raise the Williamson number, suggesting a decrease in the velocity field. Figure 6 depicts how the profile of f″(η) in the solution uplifts owing to W. Figure 5 depicts the decline velocity formulation for η < 1.5 and upsurge velocity

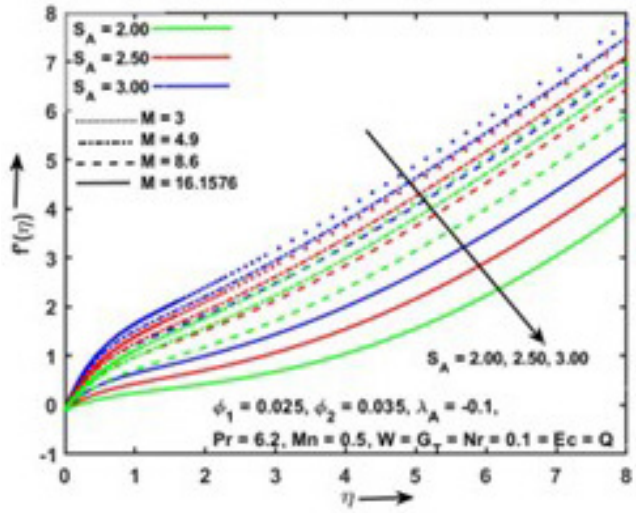


Figure 2: The formation of M and $S_A f'(\eta)$ field.

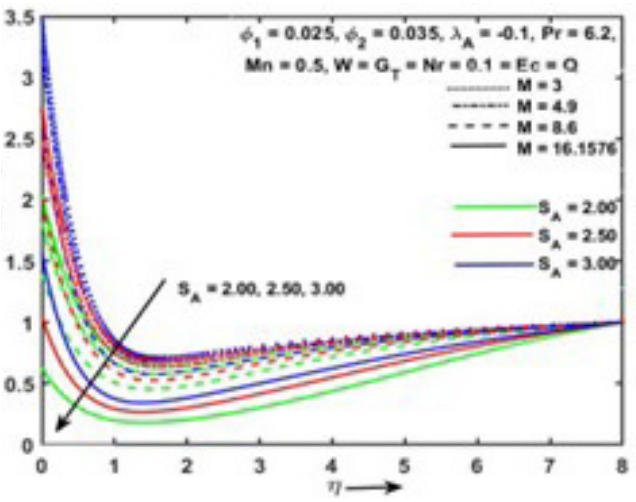


Figure 3: The formation of M and $S_A f''(\eta)$ field.

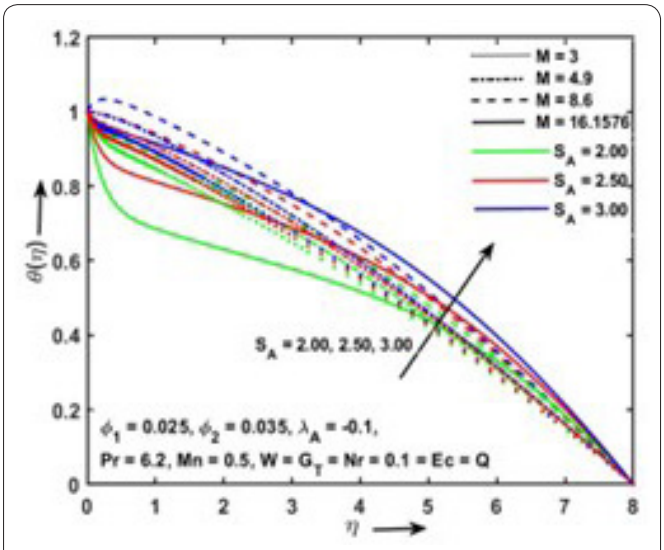


Figure 4: The formation of M and of $S_A \theta(\eta)$ field.

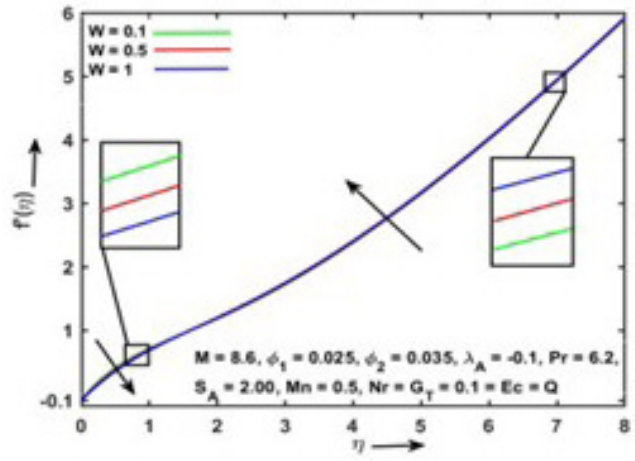


Figure 5: The formation of $Wf'(\eta)$ field.

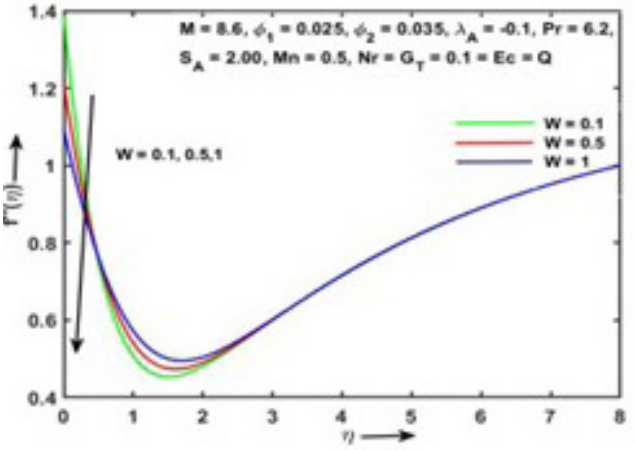


Figure 6: The formation of $Wf''(\eta)$ field.

formulation for η > 1.5 of the growing W. Figure 7 to figure 9 show the impact of GT on f′(η), f″(η) and temperature profiles dispersed throughout the full spatial domain for solution vs the pseudo-similarity variable η, respectively. As can be seen in figure 7, the velocity profile grows larger in favor of larger values of G_T. Augmentation in G_T quantities ($G_T > 0$) tends to create buoyancy forces in the flow zone, which accelerate the motion of viscoelastic CuO-TiO_2/water hybrid nano-liquid at the side of the surface. Figure 8 depicts how the profile of f″(η) uplifts owing to G_T. Figure 9 shows that the relationship between temperature and Grashof number G_T is the same, i.e., the big value of Grashof number Gr causes an increase in temperature distribution (Figure 9).

Figure 10 to figure 12 depict the effect of Mn on f′(η), f″(η), and temperature formulation vs the pseudo-similarity variable η, respectively. Higher magnetic field levels resulted in increasing frictional forces, which forced the fluid velocity (Figure 10) to decrease. The temperature (Figure 12) is increased by reason of Lorentz production induced by increasing magnetic field parameter values. Furthermore, the magnetic field parameter increases the temperature because a considerable quantity of energy is stored in the fluid. When the magnetic parameter Mn grows, the solution in figure 11 also

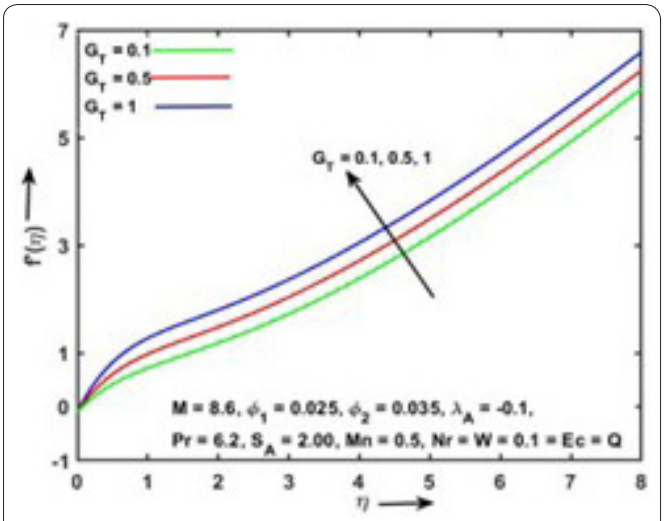


Figure 7: The formation of $G_T f'(\eta)$ field.

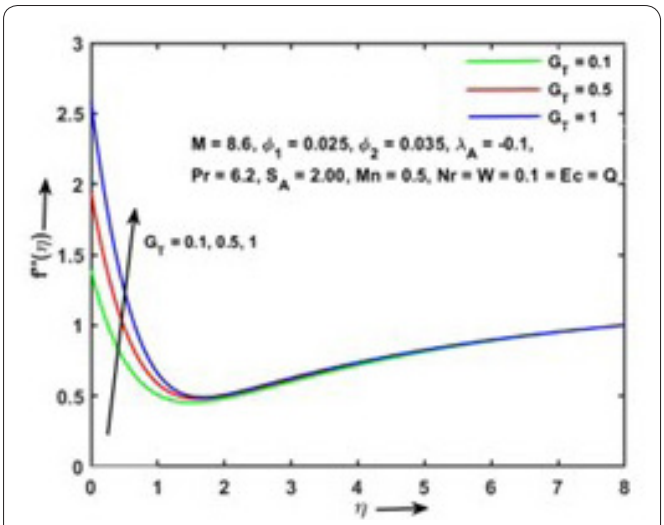


Figure 8: The formation of $G_T f''(\eta)$ field.

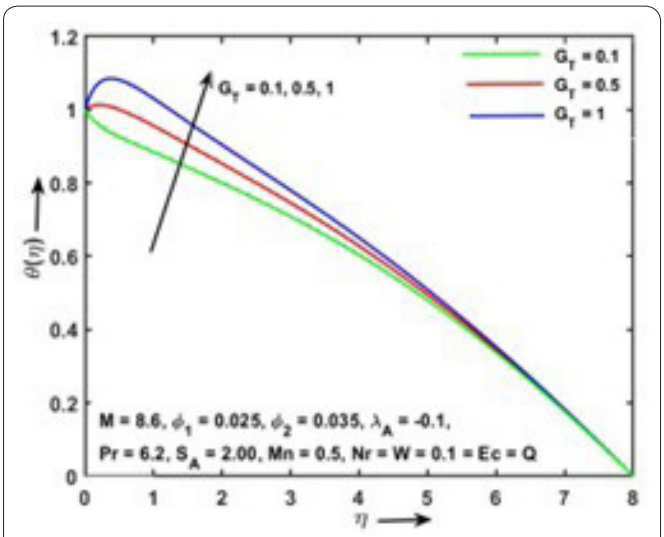


Figure 9: The formation of $G_T \theta(\eta)$ field.

describes the growing shear stress. Figures 13 to figure 15 depict the effect of S_A on f′(η), f″(η), and temperature formulation

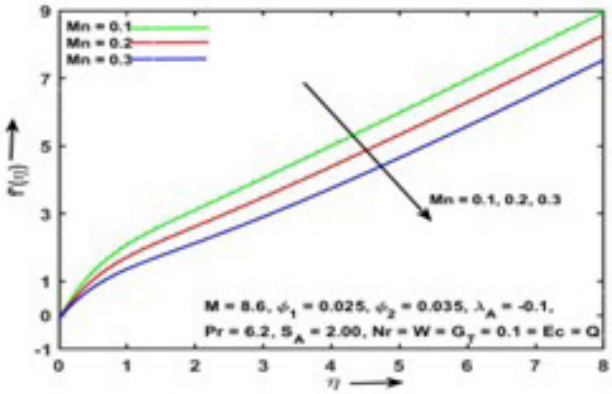


Figure 10: The formation of Mn f ' (η) field.

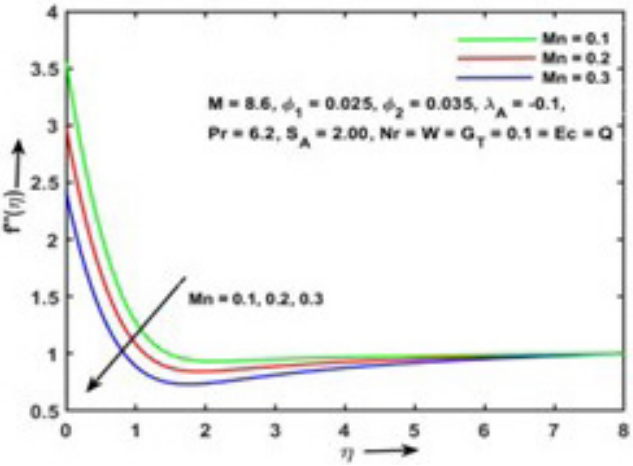


Figure 11: The formation of Mn f '' (η) field.

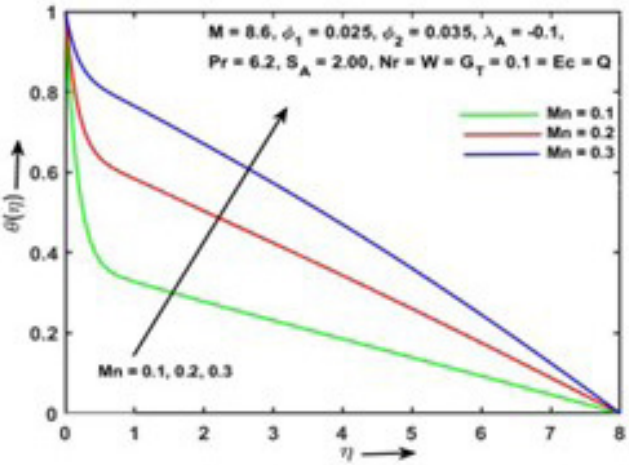


Figure 12: The formation of Mn θ (η) field.

dispersed throughout the full boundary layer section of the TiO_2-CuO/water fluid vs the pseudo-similarity variable η, respectively. As can be observed in the figure 13, the velocity components improve as the suction parameter S_A is increased, resulting in a narrower momentum barrier layer. The influence of the suction parameter S_A raises the temperature graphs, and consequently, the thickness of the thermal boundary layer. In this area, the normalised momentum barrier layer is thicker. In

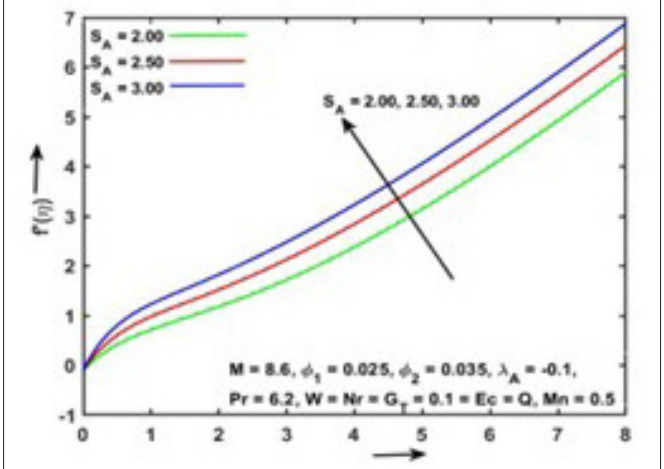


Figure 13: The formation of S_A f ' (η) field.

addition, the solution holds the normalised velocity profile's convergence criteria at infinity (Figure 14). Figure 16 to figure 18 depict the effect of λ_A on f'(η), f''(η), and temperature formulation dispersed throughout the full spatial domain for solution versus the pseudo-similarity variable η, respectively. In figure 17, the shear tress upsurges, while opposite flow is shown in figure 16 and figure 18.

Figures 19 to figure 21 depict the effect of temperature of Nr, Q, and Ec dispersed throughout the full spatial domain for solution versus the pseudo-similarity variable η, respectively. Figure 19 depicts the upsurge velocity formulation for η < 0.7 and decline velocity formulation for η > 0.7 of the growing Nr. The influence of the growing Nr, which enhances thermal conductivity, causes the heat rate of flow at the surface to accelerate. As a result, temperature profiles emerge in the boundary layer area. Consequently, of the increased influence of Nr, the thermal boundary layer fatness improves. Figure 20 depicts the impact of the heat source factor Q on the non-dimensional temperature distribution. Temperature rises when the strength of the heat source fluid grows owing to an increasing thickness of the thermal boundary. Figure 21 displays the nature of thermal graphs for many values of the Eckert number Ec. Practically, a rise in Ec enhances fluid friction, which causes fluid particles to collide more frequently, generating heat energy in the medium. As a result, as the Eckert number is enlarged, the width of the thermal boundary layer grows.

Figures 22 to figure 24 depict the effect of $\phi_1 = \phi_2$ on f'(η), f''(η), and temperature formulation dispersed throughout the full spatial domain versus the pseudo-similarity variable η, respectively. Figure 24 shows the upsurge temperature profiles in response to the substantial influence of equal volume fraction of nanomaterials (i.e., $\phi_1 = \phi_2$). On nanoparticles, the temperature profiles and volumetric fractions follow the law of direct connection. As a result of the larger influence of ϕ_1 and ϕ_2, the temperature is displaying an upsurge behaviour. Furthermore, because of the greater nanomaterial volumetric fractions, the thermal conductivity of the hybrid nano-liquid enlarges, subsequent in a quicker heat transfer rate in response to changing temperature profiles. While the velocity and shear stress profiles reduced with upsurge $\phi_1 = \phi_2$.

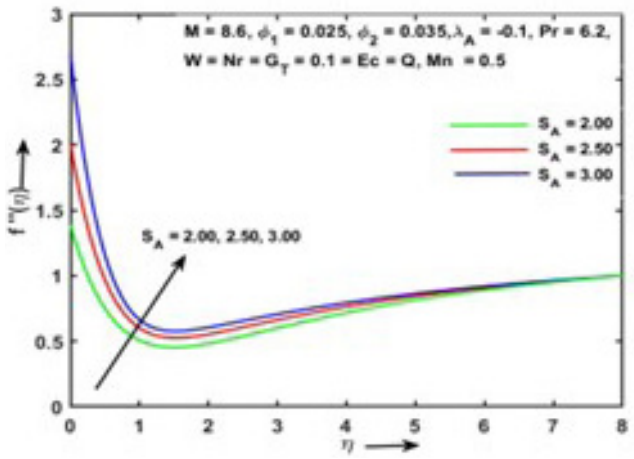


Figure 14: The formation of S_A f " (η) field.

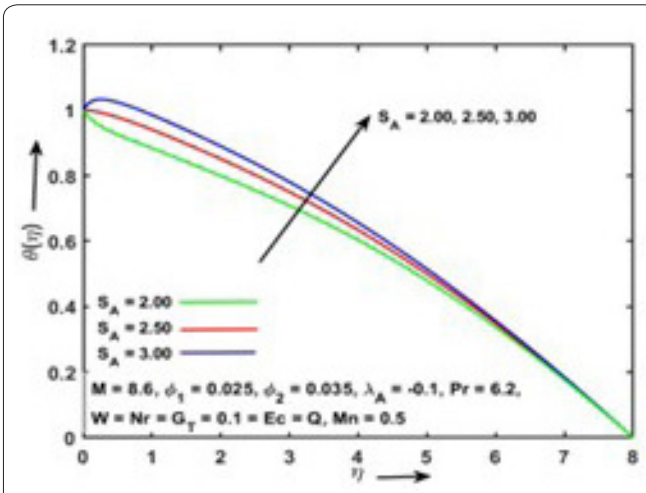


Figure 15: The formation of S_A θ (η) field.

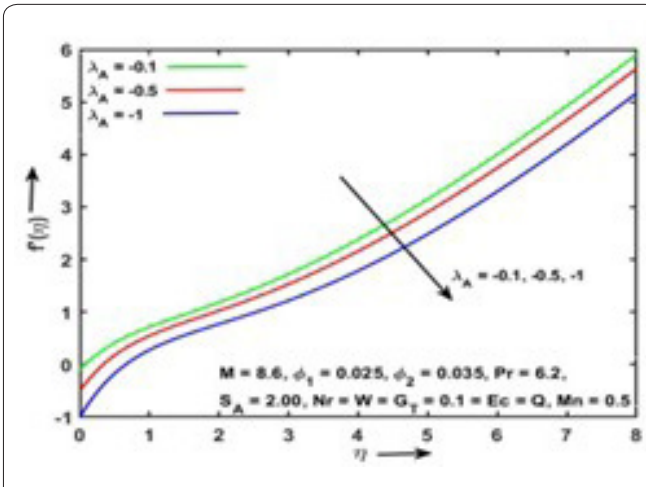


Figure 16: The formation of λ_A f ' (η) field.

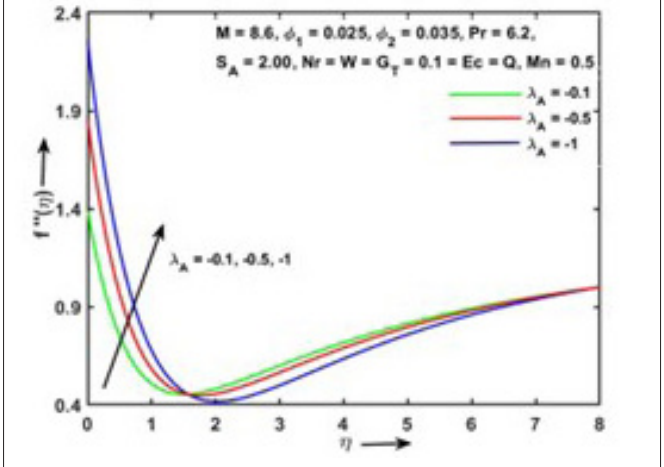


Figure 17: The formation of λ_A f " (η) field.

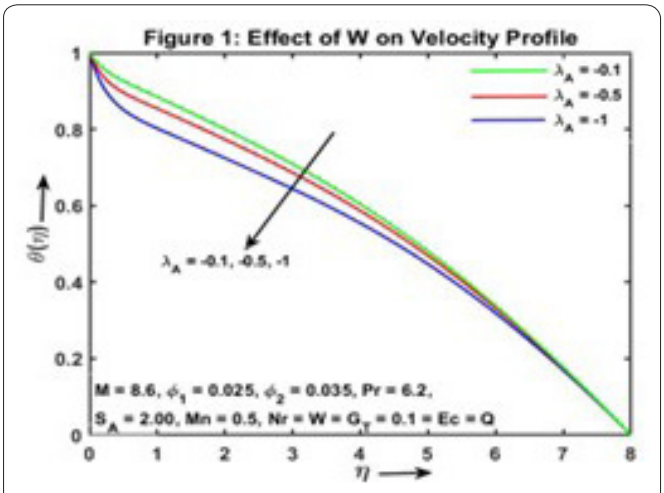


Figure 18: The formation of λ_A θ (η) field.

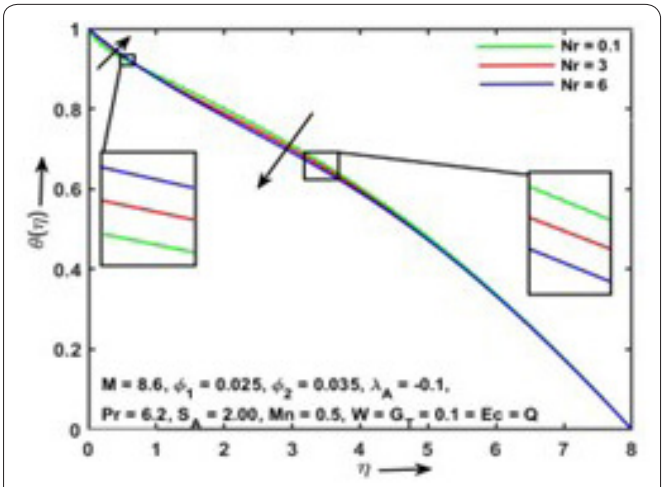


Figure 19: The formation of Nr θ (η) field.

Figure 25 to figure 27 depict the velocity, shear stress, and temperature shapes of increasing volume fractions of CuO and TiO_2 nanoparticles. In which, we see the temperature formulation increases while opposite behaviors are shown for velocity and shear stress formulations. Table 4 shows the skin-friction and Nusselt number impressions with dimensionless parameters.

The findings of the shear stress for the limited situation of the reducing parameter λ_A < 0 have been coordinated with the outcomes of [12, 25] to support the validity, correctness, and exactness of the careful mathematical system. The mathematical results are provided in table 5, which shows an amazing fit and harmony with the available results, giving

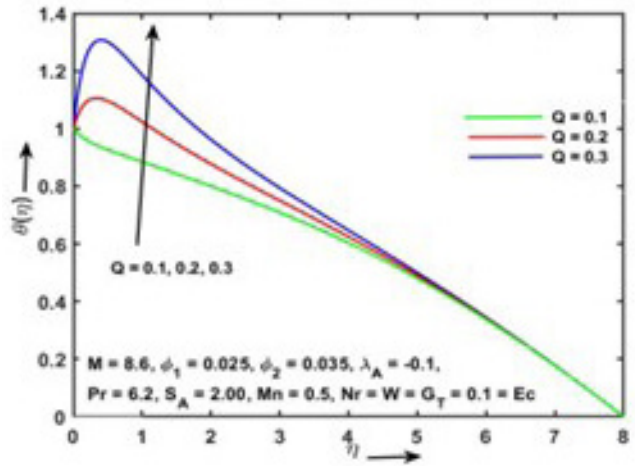


Figure 20: The formation of Q_θ (η)field.

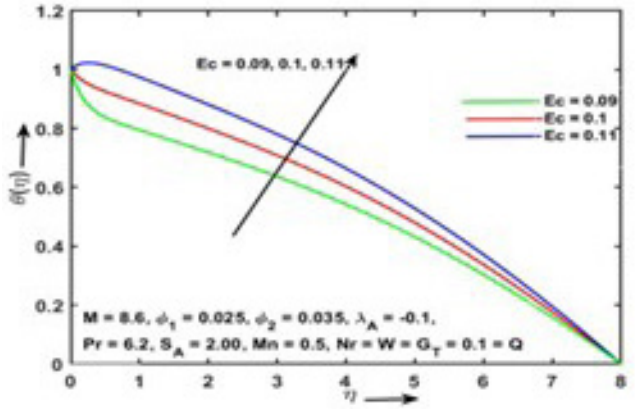


Figure 21: The formation of Ec θ (η) field.

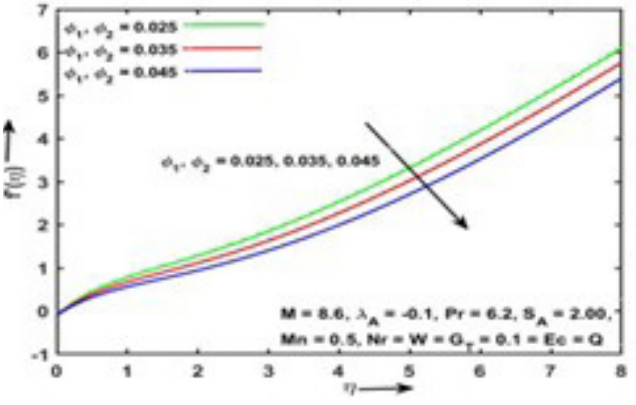


Figure 22: The formation of ϕ_{CuO}, ϕ_{TiO_2} f'(η) field.

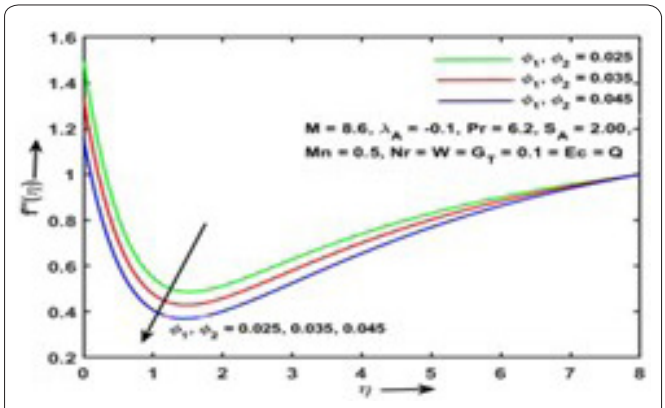


Figure 23: The formation of ϕ_{CuO}, ϕ_{TiO_2} f "(η) field.

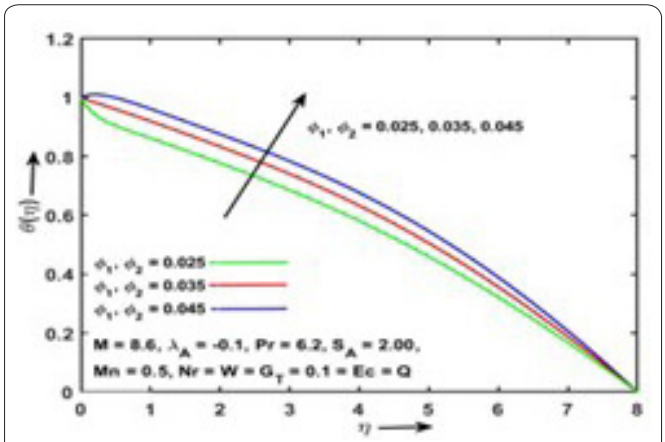


Figure 24: The formation of $\phi_{CuO}, \phi_{TiO_2} \theta(\eta)$ field.

us further confidence that the results in the current study are quite exact.

Conclusions

The latest research-validated numerical research on heat transference and crossflow of Williamson fluid over a porous reducing sheet using the Weissenberg, Hartmann, local Grashof temperature, Eckert, heat source/sink, and Prandtl, radiation, and shape factors assigning hybrid nanofluid. The findings demonstrate that a hybrid nano-solution is possible, which may be described by using certain influencing factors.

- Only when the sheet shrinks to a particular size do the answer show.
- The friction coefficient is reduced, and the heat transference rate efficacy is improved as the volume fraction of nano materials increases in a hybrid nanofluid flow.
- Improving Q and Ec increased the heat transference rate, but growing Pr and Nr had the reverse effect.
- The friction factor increased as GT and SA improved, but increasing W and Mn had the reverse effect.
- In the future, we will expand this flow model to include the various types of geometry like as Riga plate, cylindrical sheet etc and the convective heating scenario.

Acknowledgements

None.

Conflict of Interest

None.

Table 4: Impacts of ϕ_{CuO}, ϕ_{TiO_2}, λ_A, W, S_A, Nr, Q, Ec, G_T, Mn, and R, quantitative values of $C_f \mathrm{Re}_x^{1/2}$ and $C_f \mathrm{Re}_x^{1/2}$.

S_A	λ_A	W	Mn	$C_f \mathrm{Re}_x^{1/2}$	$Nu_x \mathrm{Re}_x^{-1/2}$
2	-0.1	0.1	0.5	1.73317	0.43327
2.5				2.582	-0.0192
3				3.56644	-0.5836
2	-0.1	0.1	0.5	1.73317	0.43327
	-0.5			2.35976	0.67686
	-1			2.93127	0.97083
2	-0.1	0.1	0.5	1.73317	0.43327
		0.5		1.84077	0.39192
		1		1.97713	0.33341
2	-0.1	0.1	0.1	4.89402	5.34086
			0.2	4.00077	3.0293
			0.3	3.16939	1.43448
G_T	Pr	Nr	Ec	$C_f \mathrm{Re}_x^{1/2}$	$Nu_x \mathrm{Re}_x^{-1/2}$
0.1	6.2	0.1	0.1	1.73317	0.43327
0.5				2.49073	-0.2373
1				3.41279	-0.9735
0.1	5	0.1	0.1	1.73307	0.38289
	10			1.73333	0.59638
	15			1.73343	0.8055
0.1	6.2	0.1	0.1	1.73317	0.43327
		3		1.73224	0.88551
		6		1.73146	1.36519
0.1	6.2	0.1	0.09	1.71559	1.2169
			0.1	1.73317	0.43327
			0.11	1.75073	-0.3541
Q	ϕ_{CuO}	ϕ_{TiO_2}	M	$C_f \mathrm{Re}_x^{1/2}$	$Nu_x \mathrm{Re}_x^{-1/2}$
0.1	0.025	0.035	8.6	1.73317	0.43327
0.2				1.75499	-1.3102
0.3				1.7803	-3.4279
0.1	0.025	0	8.6	2.07156	1.2556
	0.035			2.08159	0.87879
	0.045			2.08976	0.509
0.1	0	0.025	8.6	1.87789	1.50555
		0.035		1.81327	1.26291
		0.045		1.74863	1.0397

Table 5: In the absence of ϕ_{CuO}, ϕ_{TiO_2}, λ_A, W, S_A, Nr, Q, Ec, G_T, Mn, and R, quantitative values of $C_f \mathrm{Re}_x^{1/2}$ for shrinkage parameter $\lambda_A < 0$.

λ_A	Waini et al. [12]	Khan et al. [13]	**Existing resolution**
-0	0.99344	0.9934458	0.993440171
-0	0.971925	0.97192345	0.971924635
-0	0.931424	0.93142134	0.931423695
-0	0.864452	0.86445098	0.864452596
-1	0.752585	0.75258346	0.75258471

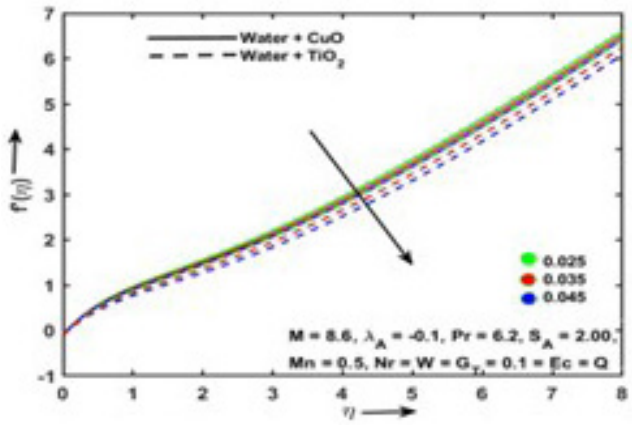


Figure 25: The formation of $water + \phi_{CuO}, water + \phi_{TiO_2} \mathrm{f}'(\eta)$ field.

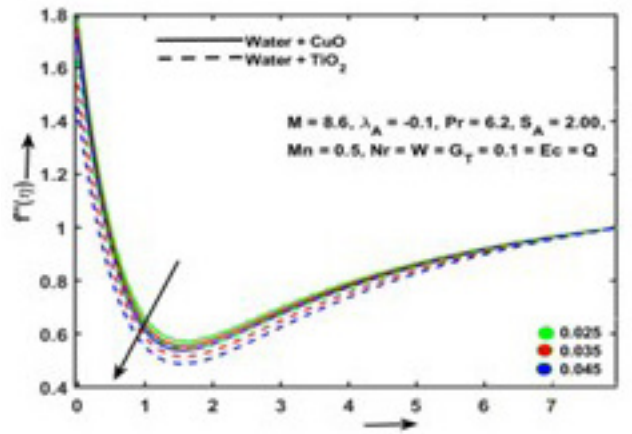


Figure 26: The formation of $water + \phi_{CuO}, water + \phi_{TiO_2} \mathrm{f}''(\eta)$ field.

References

1. Weidman PD, Kubitschek DG, Brown SN. 1997. Boundary layer similarity flow driven by power-law shear. *Acta Mech* 120: 199-215. https://doi.org/10.1007/BF01174324
2. Labib MN, Nine MJ, Afrianto H, Chung H, Jeong H. 2013. Numerical investigation on effect of base fluids and hybrid nanofluid in forced convective heat transfer. *Int J Therm Sci* 71: 163-171. https://doi.org/10.1016/j.ijthermalsci.2013.04.003
3. Madhesh D, Kalaiselvam S. 2014. Experimental analysis of hybrid nanofluid as a coolant. *Procedia Eng* 97: 1667-1675. https://doi.

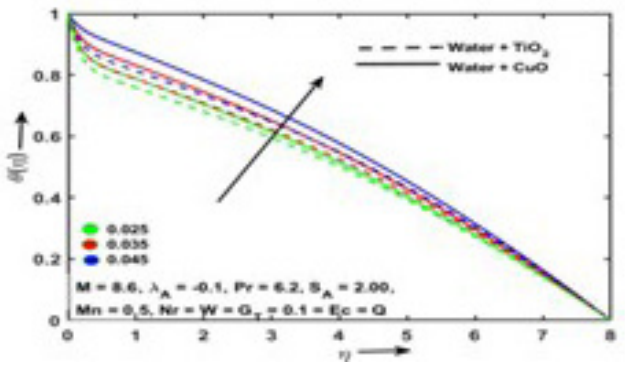


Figure 27: The formation of $water + \phi_{CuO}, water + \phi_{TiO_2}\theta(\eta)$ field.

org/10.1016/j.proeng.2014.12.317

4. Sarkar J, Ghosh P, Adil A. 2015. A review on hybrid nanofluids: recent research, development and applications. *Renew Sust Energ Rev* 43: 164-177. https://doi.org/10.1016/j.rser.2014.11.023
5. Kareem AK, Mohammed HA, Hussein AK, Gao S. 2016. Mixed convection heat transfer in a lid-driven trapezoidal enclosure filled with nanofluids. *Int Commun Heat Mass Transf* 3482.
6. Babu JR, Kumar KK, Rao SS. 2017. State-of-art review on hybrid nanofluids. *Renew Sust Energy Rev* 77: 551-565. https://doi.org/10.1016/j.rser.2017.04.040
7. Nabil MF, Azmi WH, Hamid KA, Zawawi NN, Priyandoko G, et al. 2017. Thermo-physical properties of hybrid nanofluids and hybrid nanolubricants: a comprehensive review on performance. *Int Commun Heat Mass Transf* 83: 30-39. https://doi.org/10.1016/j.icheatmasstransfer.2017.03.008
8. Sidik NA, Jamil MM, Japar WM, Adamu IM. 2017. A review on preparation methods, stability and applications of hybrid nanofluids. *Renew Sust Energy Rev* 80: 1112-1122. https://doi.org/10.1016/j.rser.2017.05.221
9. Esfe MH, Amiri MK, Alirezaie A. 2018. Thermal conductivity of a hybrid nanofluid. *J Therm Anal Calorim* 134(2): 1113-1122. https://doi.org/10.1007/s10973-017-6836-9
10. Vasanthakumari R, Pondy P. 2018. Mixed convection of silver and titanium dioxide nanofluids along inclined stretching sheet in presence of MHD with heat generation and suction effect. *Math Model Eng Probl* 5(2): 123-129. https://doi.org/10.18280/mmep.050210
11. Mostafazadeh A, Toghraie D, Mashayekhi R, Akbari OA. 2019. Effect of radiation on laminar natural convection of nanofluid in a vertical channel with single-and two-phase approaches. *J Therm Anal Calorim* 138(1): 779-794. https://doi.org/10.1007/s10973-019-08236-2
12. Waini I, Ishak A, Pop I. 2019. Unsteady flow and heat transfer past a stretching/shrinking sheet in a hybrid nanofluid. *Int J Heat Mass Transf* 136: 288-297. https://doi.org/10.1016/j.ijheatmasstransfer.2019.02.101
13. Khan U, Zaib A, Sheikholeslami M, Wakif A, Baleanu D. 2020. Mixed convective radiative flow through a slender revolution bodies containing molybdenum-disulfide graphene oxide along with generalized hybrid nanoparticles in porous media. *Crystals* 10(9): 771. https://doi.org/10.3390/cryst10090771
14. Khan U, Zaib A, Khan I, Nisar KS. 2020. Dual solutions of nanomaterial flow comprising titanium alloy (Ti6Al4V) suspended in Williamson fluid through a thin moving needle with nonlinear thermal radiation: stability scrutinization. *Sci Rep* 10(1): 20933. https://doi.org/10.1038/s41598-020-77996-x
15. Qureshi MA. 2020. Numerical simulation of heat transfer flow subject to MHD of Williamson nanofluid with thermal radiation. *Symmetry* 13(1): 10. https://doi.org/10.3390/sym13010010
16. Asadi A, Alarifi IM, Foong LK. 2020. An experimental study on characterization, stability and dynamic viscosity of CuO-TiO_2/water hybrid nanofluid. *J Mol Liq* 307: 112987. https://doi.org/10.1016/j.molliq.2020.112987
17. Aziz A, Jamshed W, Ali Y, Shams M. 2020. Heat transfer and entropy analysis of Maxwell hybrid nanofluid including effects of inclined magnetic field, Joule heating and thermal radiation. *Discret Contin Dyn Syst S* 13: 2667. https://doi.org/10.3934/dcdss.2020142
18. Chu YM, Nisar KS, Khan U, Daei Kasmaei H, Malaver M, et al. 2020. Mixed convection in MHD water-based molybdenum disulfide-graphene oxide hybrid nanofluid through an upright cylinder with shape factor. *Water* 12(6): 1723. https://doi.org/10.3390/w12061723
19. Nisar KS, Khan U, Zaib A, Khan I, Baleanu D. 2020. Exploration of aluminum and titanium alloys in the stream-wise and secondary flow directions comprising the significant impacts of magnetohydrodynamic and hybrid nanofluid. *Crystals* 10(8): 679. https://doi.org/10.3390/cryst10080679
20. Date MK, Yang LH, Yang TY, Wang KY, Su TY, et al. 2020. Three-dimensional CuO/TiO_2 hybrid nanorod arrays prepared by electrodeposition in AAO membranes as an excellent fenton-like photocatalyst for dye degradation. *Nanoscale Res Lett* 15: 45. https://doi.org/10.1186/s11671-020-3266-6
21. Albeshri BA, Islam N, Bokhary AY, Pasha AA. 2021. Hydrodynamic analysis of laminar mixed convective flow of Ag-TiO_2-water hybrid nanofluid in a horizontal annulus. *CFD Lett* 13(7): 47-57. https://doi.org/10.37934/cfdl.13.7.4557
22. Ramzan M, Dawar A, Saeed A, Kumam P, Watthayu W, et al. 2021. Heat transfer analysis of the mixed convective flow of magnetohydrodynamic hybrid nanofluid past a stretching sheet with velocity and thermal slip conditions. *PLoS One* 16(12): e0260854. https://doi.org/10.1371/journal.pone.0260854
23. Muhammad K, Hayat T, Alsaedi A, Ahmad B. 2021. Melting heat transfer in squeezing flow of basefluid (water), nanofluid (CNTs + water) and hybrid nanofluid (CNTs + CuO + water). *J Therm Anal Calorim* 143: 1157-1174. https://doi.org/10.1007/s10973-020-09391-7
24. Othman MN, Jedi A, Bakar NA. 2021. MHD flow and heat transfer of hybrid nanofluid over an exponentially shrinking surface with heat source/sink. *Appl Sci* 11(17): 8199. https://doi.org/10.3390/app11178199
25. Khan U, Zaib A, Bakar SA, Ishak A, Baleanu D, et al. 2022. Computational simulation of cross-flow of Williamson fluid over a porous shrinking/stretching surface comprising hybrid nanofluid and thermal radiation. *AIMS Math* 7(4): 6489-6515. https://doi.org/10.3934/math.2022362
26. Almaneea A. 2022. Numerical study on heat and mass transport enhancement in MHD Williamson fluid via hybrid nanoparticles. *Alex Eng J* 61(10): 8343-8354. https://doi.org/10.1016/j.aej.2022.01.041